

Modification of Proton Velocity Distributions by Alfvénic Turbulence in the Solar Wind

V. Pierrard^{1,2} · Y. Voitenko¹ ·

Received ; accepted

© Springer ●●●

Abstract In the present paper, the proton velocity distribution function (VDF) in the solar wind is determined by solving numerically the kinetic evolution equation. We compare the results obtained when considering the effects of external forces and Coulomb collisions with those obtained by adding effects of Alfvén wave turbulence. We use Fokker-Planck diffusion terms due to Alfvénic turbulence, which take into account observed turbulence spectra and kinetic effects of finite proton gyroradius. Assuming a displaced Maxwellian for the proton VDF at the simulation boundary at 14 solar radii, we show that the turbulence leads to a fast (within several solar radii) development of the anti-sunward tail in the proton VDF. Our results provide a natural explanation for the nonthermal tails in the proton VDFs, which are often observed in-situ in the solar wind beyond 0.3 AU.

Keywords: Solar wind; Waves; Turbulence; Space Plasmas

1. Introduction

The solar wind is a low density plasma in which kinetic processes prevail. Kinetic models based on the solution of the Fokker-Planck equation have been developed to study the steady state electron velocity distribution function (VDF) in the corona and at larger radial distances in the solar wind (SW) (Lie-Svendsen *et al.*, 1997; Pierrard *et al.*, 1999; Lie-Svendsen and Leer, 2000; Pierrard *et al.*, 2001; Vocks and Mann, 2003; Vocks and Mann, 2009). The test electrons were submitted to the influence of the external forces and to Coulomb collisions with background particles (Pierrard *et al.*, 1999; Lie-Svendsen and Leer, 2000; Pierrard *et al.*, 2001). Such models were solved numerically and emphasized the effects of Coulomb collisions compared to the results of purely exospheric models that considered only the external forces

¹ Solar-Terrestrial Centre of Excellence, Space Physics, Belgian Institute for Space Aeronomy, Ringlaan 3 av. Circulaire, B-1180 Brussels, Belgium, email: viviane.pierrard@oma.be

² Georges Lemaître Centre for Earth and Climate Research (TECLIM), Université Catholique de Louvain, Place Louis Pasteur 3, bte L4.03.08, 1348 Louvain-la-Neuve, Belgium

(Maksimovic *et al.*, 1997; Lamy *et al.*, 2003). They showed that Coulomb collisions have important effects on angular scattering (*i.e.* on the pitch angle distribution of the electrons) but do not modify their average density and mean temperatures radial distributions. Models including Coulomb collisions gave more realistic VDFs and a reduction of the temperature anisotropies compared to the purely exospheric approximation (Lemaire and Pierrard, 2001), because the Coulomb collisions isotropize the electron VDF. Terms due to whistler wave turbulence have also been included in the electron kinetic equation and its influence on the formation of nonthermal tails and on the velocity-space diffusion of electrons has been investigated (Pierrard *et al.*, 2011).

In the present paper, we study the evolution of the proton VDF in the solar wind. First, we use a kinetic approach similar to the mentioned above papers, which accounts for the effects on the protons of the external forces and Coulomb collisions. After that we include also the wave effects on the proton VDF. Recent in-situ measurements have revealed that the wave activity at the proton kinetic scales is dominated by Alfvén waves rather than whistlers (He *et al.*, 2011; He *et al.*, 2012; Podesta and Gary, 2011). Among Alfvén waves, the most power, about 80%, is in highly oblique kinetic Alfvén waves (KAWs), and the rest 20% is in quasi-parallel ion-cyclotron Alfvén mode (He *et al.*, 2011). Both the MHD-scale and kinetic-scale Alfvén waves possess power law spectral distributions and exhibit turbulence properties. We therefore use in present simulations a 1D-2D (1D spatial - 2D velocity-space) Fokker-Planck diffusion term due to Alfvénic turbulence derived by Voitenko and Pierrard (2012).

Voitenko and Goossens (2006) suggested that the proton trapping in the parallel KAW potential can be responsible for the proton beams observed in the solar wind. Later on, at the Solar Wind 12 in June 2009, Pierrard and Voitenko have presented analytical estimations and numerical example, published in Pierrard and Voitenko (2010). Numerical simulations by Osmane *et al.* (2010) and Li *et al.* (2010) have demonstrated the proton beam formation by a coherent monochromatic KAW. Our present approach is based not on monochromatic KAWs but on a wide spectrum of KAWs with overlapping potentials, which results in the velocity-space proton diffusion rather than the proton trapping as in the mentioned above papers.

2. Description of the Model

The kinetic transport equation for the evolution of the velocity distribution function $f(\mathbf{r}, \mathbf{v}, t)$ of the protons in the SW is given by:

$$\frac{\partial f(\mathbf{r}, \mathbf{v}, t)}{\partial t} + (\mathbf{v} \cdot \nabla_{\mathbf{r}})f(\mathbf{r}, \mathbf{v}, t) + (\mathbf{a} \cdot \nabla_{\mathbf{v}})f(\mathbf{r}, \mathbf{v}, t) = \left(\frac{df}{dt}\right)_C + \left(\frac{df}{dt}\right)_A \quad (1)$$

where \mathbf{r} and \mathbf{v} are respectively the position and velocity vectors of the particles, \mathbf{a} is the acceleration due to external forces and t is the time. We are interested by the steady state solution of this equation. The right-hand-side represents the interactions between the particles. In the present paper, we consider the Coulomb

collisions with the Fokker-Planck term $\left(\frac{df}{dt}\right)_C$ and wave-particle interactions with kinetic Alfvén waves $\left(\frac{df}{dt}\right)_A$.

In the case of the SW, the forces are the electric force $Ze\mathbf{E}$, the gravitational force $m\mathbf{g}$ and the Lorentz force resulting from the magnetic field distribution. The acceleration term for the protons is thus given by:

$$\mathbf{a} = \left(\frac{Ze\mathbf{E}}{m} + \mathbf{g}\right) + \frac{Ze}{m}(\mathbf{v} \times \mathbf{B}) = \mathbf{a}_r(r) + \mathbf{a}_L \quad (2)$$

where Ze is the electric charge of the protons ($Z = 1$), m their mass, \mathbf{E} the electric field, \mathbf{g} the gravitational acceleration, \mathbf{B} the magnetic field (assumed to decrease as r^{-2}), $\mathbf{a}_r(r)$ is the radial component of the acceleration due to the electric and gravitational forces that are vertical and \mathbf{a}_L is the non radial term due to the Lorentz force.

The simplest solar wind models consider only the effects of these external forces. In such models called exospheric, the interaction terms in Equation (1) are neglected so that an analytic solution of the equation can be obtained.

Figure 1 shows the profiles of the VDF moments obtained with the exospheric solar wind model developed by Pierrard and Lemaire (1996) and improved by Maksimovic *et al.* (1997) and Lamy *et al.* (2003). In such models, truncated Maxwellian and Kappa VDF are assumed respectively for the protons and the electrons with given density and temperatures at the exobase level (here chosen to be at $1.5 R_s$ (solar radius)). The VDF is obtained at larger radial distance by solving the evolution equation, *i.e.* Equation (1) without interaction right-hand-side terms.

It can be seen (Figure 1d) that the particles are accelerated at low radial distances due to the effects of the external forces. It is mainly from 1 to $20 R_s$ that the bulk velocity of the particle increases and then it becomes almost constant at higher radial distances. This result is similar to that obtained in MHD solar wind models where the interactions between the particles are taken into account (Parker, 1958).

The exospheric model emphasizes that it is the electrostatic potential (see Figure 1b) that increases the velocity of the particles. This potential ensures that the proton flux is everywhere equal to that of the electrons so that no net current is transported by the solar wind.

In this model, the acceleration is reinforced by the presence of suprathermal electrons simulated by a Kappa VDF. They increase the electrostatic potential and thus accelerate the wind. On the contrary, the presence of suprathermal protons has almost no influence on the electrostatic potential (Maksimovic *et al.*, 1997). That is why a Maxwellian is assumed at the reference level for the proton VDF at $1.5 R_s$. The averaged values of the different moments (profiles of number density, bulk velocity, temperatures) are in good agreement with the solar wind observations, except the temperature anisotropies that are too high in the model and would be expected to produce plasma instabilities in the system. Such high anisotropies are mainly due to the assumption of magnetic moment conservation for each particle species that is not realistic, even in low density plasmas.

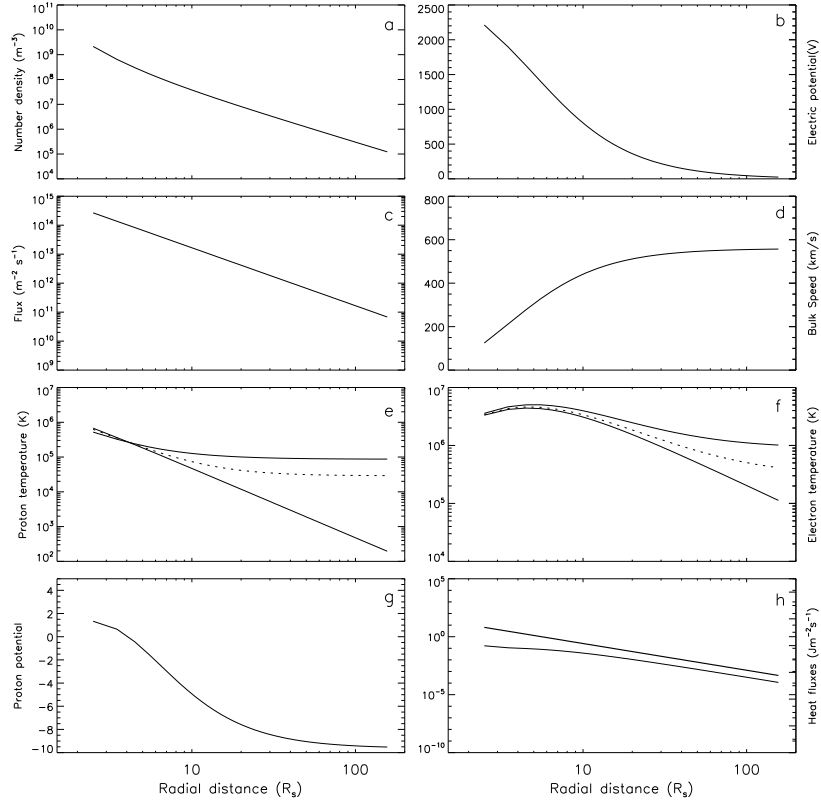


Figure 1. Profiles of (a) number density, (b) electric potential, (c) flux, (d) bulk speed, (e) proton temperature T_p (upper solid line: T_{\parallel} , bottom solid line: T_{\perp} , dotted line: average T), (f) electron temperature (*idem*), (g) proton potential, and (h) heat flux (upper and lower curves for electrons and protons) from $r_0=1.5 R_{\odot}$ up to $200 R_{\odot}$ obtained with a kinetic exospheric model of the solar wind with $T_e = 1.5 \times 10^6$ K and $T_p = 1.5 \times 10^6$ K for a Maxwellian proton VDF and a Kappa electron VDF with $\kappa=3$.

3. Numerical Model

More sophisticated solar wind models including interaction terms (the right-hand-side of Equation (1)) need to be solved numerically. We develop in the present paper such a numerical model for the protons, based on similar assumptions as those used for the model of SW electrons (Pierrard *et al.*, 1999).

We simplify the equation by using only three coordinates: the radial distance r , the velocity v and $\eta = \cos\theta = \hat{\mathbf{B}}_0 \cdot \hat{\mathbf{k}}$ where θ is the pitch angle between the velocity vector and the magnetic field direction assumed to be radial. The

left-hand-side of Equation (1) becomes:

$$Df = \frac{\partial f}{\partial t} + v\eta \frac{\partial f}{\partial r} + a_r(r) \left(\eta \frac{\partial f}{\partial v} + \frac{(1-\eta^2)}{v} \frac{\partial f}{\partial \eta} \right) + \frac{v}{r}(1-\eta^2) \frac{\partial f}{\partial \eta}. \quad (3)$$

As a first study, we will consider that the term $(df/dt)_C$ on the right-hand-side of Equation (1) represents the effects of the Coulomb collisions (Pierrard *et al.*, 2001). Then, in a next section of this paper, we adopt in addition the kinetic Alfvén wave term $(df/dt)_A$.

4. Spectral Method of Solution

To obtain steady state solutions for the proton VDF, we use a specialized spectral method similar as that described in (Pierrard, 2011) for the resolution of the Fokker-Planck equation (FPE).

The dimensionless velocity is defined by

$$x = \sqrt{\frac{m_p}{2k_B T_p(r)}} v = \frac{v}{v_{th}(r)}, \quad (4)$$

where v_{th} is the proton thermal speed and k_B is the Boltzmann constant.

The solution is expanded in terms of orthogonal polynomials:

$$f(z, x, \eta) = \exp(-x^2) \times \left(\sum_{l=0}^{J-1} \sum_{s=0}^{N-1} \sum_{m=0}^{M-1} a_{lsm} P_l(\eta) S_s(x) L_m(z) \right). \quad (5)$$

where J , N , and M are integers whose value is adjusted to obtain the required numerical precision for the solution. We use Legendre polynomials $P_l(\eta)$ with respect to $\eta = \cos \theta$, speed polynomials $S_s(x)$ with respect to the normalized velocity x and displaced Legendre polynomials on the interval $[0, c]$ with respect to the dimensionless altitude z . The a_{lsm} coefficients are the coefficients of the expansion to be determined.

The boundary condition determines the value of some coefficients a_{lsm} at the reference level. The equation is solved numerically to find the VDF $f(z, x, \eta)$ at the other radial distances. We choose 10 polynomials for each variable so that the results have a precision better than 10 % with reasonably short CPU times. We have checked that the results do not change significantly when J , N or M is increased.

The advantage of this method is that in a discrete ordinate basis, the derivatives of any continuous function $f(y)$ can be approximated by the following expansion:

$$\left(\frac{\partial f}{\partial y} \right)_{y=y_i} \approx \sum_{j=0}^{N-1} D_{ij} f(y_j) \quad (6)$$

where D_{ij} are the matrix elements of the derivative operator in the polynomial basis.

The integrals to calculate the moments of the protons are also easily performed by numerical quadrature taking into account the polynomial expansion (Pierrard and Lemaire, 1996). The moments are calculated from the VDF found by solving the FPE. The density is given by:

$$n(r) = \int f(r, v, \eta) dv. \quad (7)$$

The bulk velocity is calculated by:

$$\mathbf{u}(r) = \left(\int f(r, v, \eta) \mathbf{v} dv \right) / n. \quad (8)$$

The temperature corresponds to a second order moment of the VDF:

$$T(r) = \frac{1}{3}(T_{\parallel}(r) + 2T_{\perp}(r)) \quad (9)$$

where

$$T_{\parallel}(r) = \frac{m \int (v_{\parallel} - u)^2 f(r, v, \eta) dv}{k_{\text{B}} n(r)} \quad (10)$$

$$T_{\perp}(r) = \frac{m \int v_{\perp}^2 f(r, v, \eta) dv}{2k_{\text{B}} n(r)}. \quad (11)$$

5. The Effects of Coulomb Collisions

The effects of the binary Coulomb collisions are taken into account by using as the right-hand-side term in Equation (1) the Fokker-Planck collision operator appropriate when large-angle deflections can be neglected (Hinton, 1983):

$$\left(\frac{df}{dt} \right)_{\text{C}} = -\frac{\partial}{\partial \mathbf{v}} \cdot \left[\mathbf{A} f(\mathbf{r}, \mathbf{v}, t) - \frac{1}{2} \frac{\partial}{\partial \mathbf{v}} \cdot (\mathbf{D} f(\mathbf{r}, \mathbf{v}, t)) \right] \quad (12)$$

where \mathbf{A} is the dynamic friction vector

$$\begin{aligned} \mathbf{A} &= -4\pi \frac{Z_{\alpha}^2 Z_{\beta}^2 e^4 \ln \Lambda}{m_{\alpha}^2} \left(1 + \frac{m_{\alpha}}{m_{\beta}} \right) \\ &\times \int d\mathbf{v}' f_{\beta}(\mathbf{v}') \frac{(\mathbf{v} - \mathbf{v}')}{(v - v')^3} \end{aligned} \quad (13)$$

and \mathbf{D} is the velocity diffusion tensor

$$\begin{aligned} \mathbf{D} &= 4\pi \frac{Z_{\alpha}^2 Z_{\beta}^2 e^4 \ln \Lambda}{m_{\alpha}^2} \\ &\times \int d\mathbf{v}' f_{\beta}(\mathbf{v}') \left(\frac{\mathbf{I}}{v - v'} - \frac{(\mathbf{v} - \mathbf{v}')(\mathbf{v} - \mathbf{v}')}{(v - v')^3} \right). \end{aligned} \quad (14)$$

In Equations (13) and (14), $\ln \Lambda$ is the usual Coulomb logarithm containing the Debye screening effect: $\ln \Lambda \approx 24$. The index α corresponds to the test protons and β to the background particles, m the mass and Ze the charge of the particles, $f_\beta(v')$ is the velocity distribution function of the background particles assumed to be a displaced Maxwellian distribution since this VDF is solution of the Fokker-Planck operator.

We assume boundary conditions at a reference level here chosen to be $14 R_s$. It could be chosen at lower radial distances as well, but this distance corresponds to the region where kinetic Alfvén turbulence is supposed to have effects, so this altitude is especially appropriate for comparisons when this term included (see the next section). We assume an isotropic displaced Maxwellian for the protons VDF at this reference distance since this VDF is solution of the Fokker-Planck Coulomb collision term. The bulk velocity at this radial distance is chosen to be 470 km s^{-1} , as obtained with the exospheric model.

Figure 2 illustrates the VDFs (normalized to the thermal velocity and centered on the averaged bulk velocity) obtained at different radial distances by solving the FPE including the Coulomb collision term. The VDF is always presented in the reference frame centered at its bulk velocity. The dotted circle corresponds to $v/v_{\text{th}} = \sqrt{3/2}$.

The VDF remains close to a displaced Maxwellian at higher radial distances with a bulk velocity slightly increasing as illustrated on Figure 3b. Figure 3a illustrates the profile of the decreasing normalized number density and Figure 3c the decreasing temperature. Compared to the exospheric model, the effects of Coulomb collisions (obtained with the inclusion of the Fokker-Planck collision term and with the isotropic boundary condition) are mainly to reduce the temperature anisotropy of the particles.

The results depend on the boundary condition at the reference level. Since we start with an isotropic displaced Maxwellian at the reference level chosen to be $14 R_s$, the VDF remains close to a displaced Maxwellian at higher radial distances even if the Coulomb collisions become negligible at large radial distances. The bulk velocity increases with the radial distance due to the acceleration term and the Lorentz force slightly aligns the VDF to the magnetic field direction with the increasing radial distances.

6. Fokker-Planck Diffusion Terms due to Alfvénic Turbulence

In this section we include diffusion terms due to Alfvénic turbulence. The Alfvénic turbulence evolves towards small scales across the background magnetic field and at proton kinetic scales transforms into the turbulence of KAWs. The preliminary principles of KAWs on the formation of the proton beams have been presented by Pierrard and Voitenko (2010). The focus in this previous paper was on the proton trapping and acceleration in the electric potential carried by intermittent isolated KAWs. Here we use a model Alfvénic spectrum that corresponds to the magnetic power spectra measured in the solar wind.

The Alfvénic turbulence and related terms describing the velocity-space proton diffusion in the solar wind conditions have been presented in detail by

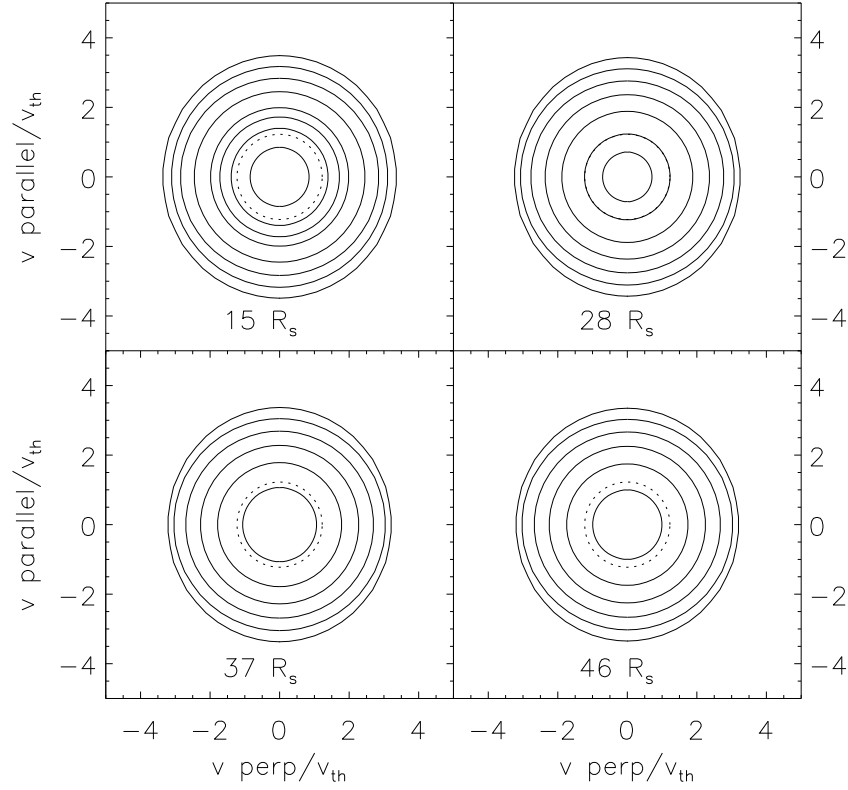


Figure 2. VDFs obtained at different radial distances assuming a displaced Maxwellian as boundary condition at $14 R_s$ by solving the FPE including the Coulomb collision term.

Voitenko and Pierrard (2012). We use here the final expressions from this paper, which are in terms of quantities measured in-situ in the solar wind. The Fokker-Planck term due to Alfvénic turbulence, which is essentially the KAW turbulence at small scales, is given by

$$\begin{aligned}
\left(\frac{\partial f_p}{\partial t}\right)_A &= \left(\eta \frac{\partial}{\partial v} + \frac{1-\eta^2}{v} \frac{\partial}{\partial \eta}\right) D_A \left(\eta \frac{\partial}{\partial v} + \frac{1-\eta^2}{v} \frac{\partial}{\partial \eta}\right) f \\
&= \eta^2 \frac{\partial}{\partial v} D_A \frac{\partial}{\partial v} f + \eta \frac{\partial}{\partial v} \frac{1-\eta^2}{v} D_A \frac{\partial}{\partial \eta} f \\
&\quad + \frac{1-\eta^2}{v} \frac{\partial}{\partial \eta} \eta D_A \frac{\partial}{\partial v} f + \frac{1-\eta^2}{v} \frac{\partial}{\partial \eta} \frac{1-\eta^2}{v} D_A \frac{\partial}{\partial \eta} f.
\end{aligned}$$

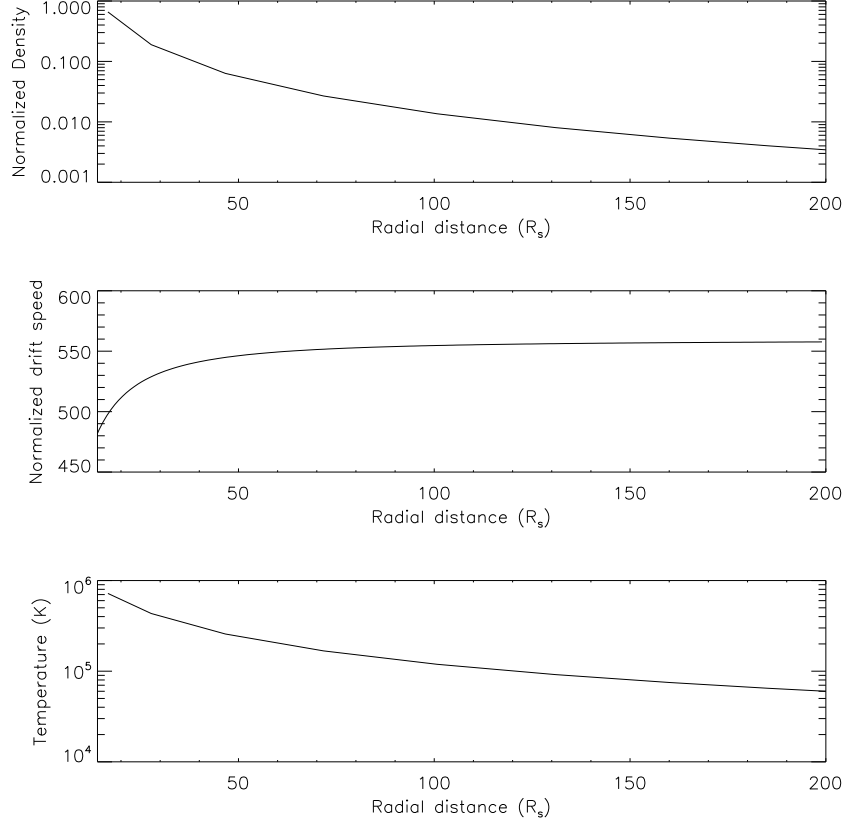


Figure 3. Radial profiles of number density, bulk velocity, and proton temperature profiles obtained by solving the FPE including the Coulomb collisions assuming a displaced Maxwellian as boundary condition at $14 R_s$.

The KAW diffusion coefficient

$$D_A = \alpha \pi^2 \Omega_p V_S V_A \frac{\left(\frac{(\eta v / V_A)^2 - 1}{2} \right)^{0.2 - 0.55((\eta v / V_A)^2 - 1) / ((\eta v / V_A)^2 + 1)}}{\left((\eta v / V_A)^2 + 1 \right) (\eta v / V_A)} \frac{|B_1|^2}{B_0^2}$$

for $1 \leq \eta v / V_A \leq \sqrt{1 + 2\mu_c^2}$, and $D_A = 0$ otherwise, where $\mu = k_\perp \rho_p$ is the perpendicular wavenumber k_\perp normalized by the proton gyroradius ρ_p . Other notations are as follows: Ω_p is the proton cyclotron frequency. V_A is the Alfvén velocity:

$$V_A (\text{cm s}^{-1}) = 2.18 \times 10^{11} \frac{B(\text{gauss})}{\sqrt{n(\text{cm}^{-3})}} \quad (15)$$

$V_S = \sqrt{k_B T_{e\parallel} / m_p}$ is the ion-acoustic velocity, and the anisotropy factor $\alpha \approx 0.3$. All the plasma parameters (background number density n_0 , parallel electron temperature $T_{e\parallel}$, and background magnetic field B_0) are functions of r .

The above expression for D_A is obtained from Equation (7) by Voitenko and Pierrard (2012) using a power-law turbulence spectrum $|B_{\mu SC}|^2 \propto |B_1|^2 \mu^{-\delta_\perp}$ with the following model for the variable index: $\delta_\perp = 1.6 + 1.1\mu^2 (1 + \mu^2)^{-1}$. This δ_\perp has the low- and high- μ asymptotes 1.6 and 2.7, as is measured in the solar wind (Alexandrova *et al.*, 2009). We also averaged D_A in the cross-field plane and put $T_e/T_p = 1$ in the KAW dispersion.

A low-beta two-fluid dispersion equation is adopted for KAWs,

$$\frac{\omega}{k_z V_A} = \sqrt{1 + \left(1 + \frac{T_{ez}}{T_{p\perp}}\right) \mu^2}, \quad (16)$$

which is a good approximation for the kinetic dispersion by Hasegawa and Chen (1976) where a possible temperature anisotropy is taken into account. A comparison among several KAW models is given by Voitenko and Pierrard (2012).

7. Formulation of the Boundary-value Problem at the Solar Wind Base

We are interested in the quasi-stationary boundary-value problem, where the MHD Alfvén waves (AWs) are injected along \mathbf{B}_0 at $r = r_0 = 14 R_S$. We assume $B(200 R_s) = 4 \text{ nT} = 4 \times 10^{-5} \text{ gauss}$ and decreasing as r^{-2} to determine B at $14 R_s$. Then d/dt means $v_z \partial / \partial r$ in the Fokker-Planck Equation (1). The nonlinear interaction of MHD AWs create MHD turbulent cascade towards smaller scales and turbulent spectra. It is found that the turbulent cascades are anisotropic and proceed mainly towards small cross-field wavelengths, where the waves are essentially kinetic Alfvén waves undergoing a wave-particle Cherenkov interaction.

As the plasma parameters, magnetic field B_0 , and Alfvén velocity V_A vary with distance, we expect that the upward propagating KAW turbulence sweeps the anti-sunward part of the particle distribution functions making them flatter or even producing a separate beam. Such distortions of the velocity distributions are often measured at the distances $\gtrsim 0.3 \text{ AU}$ (Marsch *et al.*, 1982), which can be signatures of the velocity diffusion due to the KAW turbulence.

We assume that, contrary to the distant solar wind, the Alfvénic turbulence in the vicinity of the solar wind base does not fill all the wavenumber range but evolves rapidly. We will model this by introducing a distance-dependent high-wavenumber cutoff μ_c for the spectrum of such "young", not fully developed turbulence. The turbulent spectrum in the "young" turbulence does not spread beyond $\mu = \mu_c$, but μ_c itself increases with heliocentric distance. Because of the absence of the observational data on the cutoff μ_c within 0.3 AU, we model it as

$$\mu_c = \mu_c(r) = \mu_{c0} \left(\frac{r}{r_0}\right)^3,$$

where μ_{c0} is the cutoff value at the solar wind base $r = r_0$. We assume $\mu_{c0} = 0.1$ at the boundary, such that the turbulent spectrum does not reach the proton kinetic length scales $\approx \rho_{rmp}$. The proton gyro-scale $\mu_c \approx 1$ is reached by the turbulent cascade at the distances $\approx 2r_0$.

In the near-Earth solar wind at $R = 1$ AU the normalized spectral density $|B_1|^2/B_0^2 \approx 10^{-3}$ (Alexandrova *et al.*, 2010). Since the radial dependence of $|B_1|^2/B_0^2$ is not known, we apply a self-similar projection from 1 AU to $r_0 = 14 R_S$ by keeping constant the ratio of the total turbulence energy to the spectral density at $\mu = 1$. Then we use a model profile

$$\frac{|B_1|^2}{B_0^2} = 0.05 \left[\left(\frac{r}{r_0} \right)^{-0.1} - 0.68 \right], \quad (17)$$

describing a relatively slow decrease of $|B_1|^2/B_0^2$ with r starting from $|B_1|^2/B_0^2 \approx 1.6 \times 10^{-2}$ at $r = r_0 = 14 R_S$, to $|B_1|^2/B_0^2 \approx 4 \times 10^{-3}$ at 1 AU. Alexandrova *et al.* (2010) reported values $\gtrsim 10^{-3}$ at 1 AU. This profile fits the turbulence energy in the time domains from 3 to 25 minutes, obtained by Bavassano *et al.* (1982) from Helios measurements at three radial distances between 0.3 and 1 AU. Other attempts to model the development of solar wind turbulence have adopted other turbulence profiles (Cranmer and van Ballegoijen, 2003; Cranmer *et al.*, 2007), which imply qualitatively similar turbulence behavior above $15 R_S$.

The spectral power density of magnetic fluctuations at any scale μ is $W_\mu = B_\mu^2/\mu$, where B_μ is the magnetic amplitude at that scale. The total energy of the turbulence is given by the integral over all μ from the lowest cutoff at electron scales to the largest (driving) scale at the break in the spectral index between -1 and -5/3. Most of this energy is carried by the large-scale MHD waves that compose the MHD inertial range. Formally the energy in the steep kinetic spectra of KAWs immediately available for particles is much less, of the order of $q^{-2/3}$ (here $q = k_{\perp s}/k_{\perp 1}$ is the driving-to-kinetic scale ratio, or “width” of the inertial range). The wave propagation angle at proton kinetic scales is close to $\pi/2$. Our B_1 is an average fluctuating amplitude at a particular break scale $\mu = \mu_1$ (we assumed $\mu_1=1$ for simplicity). It is therefore much smaller than the total energy of Alfvén waves at all scales.

8. Modification of Proton VDF by the Alfvénic Turbulence

It seems that the observed turbulence spectra do not evolve significantly beyond 0.3 AU, which means they are formed much closer to the Sun. Since the kinetic-scale Alfvénic turbulence and its effects on protons are our primary interest, it is convenient to set the simulation boundary at the radial distance where the turbulence cascade approaches kinetic scales. As a reference level we chose here $14 R_S$ where we allow the turbulence cascade to spread in the high-wavenumber range. Again, the solar wind is already formed in this region and the turbulence terms can be included in consideration without interfering much with the SW acceleration processes. We assume a displaced Maxwellian for the protons VDF at this reference altitude since this VDF is solution of the Fokker-Planck Coulomb

collision term. The bulk velocity at this radial distance is chosen to be 470 km s⁻¹. This choice is conventional and the boundary could be at lower or larger radial distances, which however could not change simulation results except for adjusting them to a new distance.

Figures 4-6 present results of the simulations including the turbulence terms for the radial distances starting from the simulation boundary at 14 R_s . At the boundary, the same displaced Maxwellian for protons was used as in the previous simulations. The results presented in Figure 4 show the proton VDF evolution with the radial distance. As compared to the previous simulation without turbulence, where the proton VDF remains a displaced Maxwellian at all distances, the presence of the Alfvénic turbulence in the solar wind leads to a fast development of nonthermal tails in the proton VDFs. The tails are already noticeable at the distances about one solar radius from the boundary, and they increase fast with the radial distance and become pronounced after 2-3 solar radii.

The radial behavior of the moments of the proton VDF are shown in the top panels of Figure 5. As is seen from Figure 5, the profiles of the bulk velocity and number density are also modified by the turbulence. The bulk velocity is increased in the regions where the tails are formed, and it is stabilized at higher altitudes. The number density profile decreases slower than without turbulence. The number density profile decreases less fast when the KAW amplitude B_1/B_0 is chosen to be smaller. The bottom panels of Figure 5 show the profiles of the Alfvén velocity and of the plasma beta function:

$$\beta = \left(1 + \frac{T_{\text{e}\parallel}}{T_{\text{p}\perp}}\right) \frac{V_{\text{Tp}}^2}{V_{\text{A}}^2} \quad (18)$$

where $V_{\text{Tp}} = \sqrt{k_{\text{B}}T_{\text{p}}/m_{\text{p}}}$. The most favorable conditions for the tail generation occur in the regions where the proton thermal and Alfvén velocities are about the same, *i.e.* $\beta \approx 1$.

Figure 6 illustrates the VDF obtained at 30 R_s assuming a displaced Maxwellian as boundary condition at 14 R_s by the evolution equation including the Alfvénic turbulence terms. The top panel shows the parallel (solid line) and perpendicular (dotted line) cross section of the proton VDF. It can be seen that an extended nonthermal tail is created in the direction parallel to the interplanetary magnetic field. The Coulomb collisional diffusion appeared to be efficient enough to smooth out a strong gradient at the turbulent diffusion boundary $V_z \approx V_{\text{A}}$ and to prevent formation of the quasilinear plateau at $V_z \gtrsim V_{\text{A}}$. The core distribution seems not to be affected. The bottom panel illustrates the isocontours of the proton VDF in the velocity plane centered on the bulk velocity.

Particles VDF measured in-situ in the solar wind show many non-thermal features, like particle beams, thermal anisotropies, heat fluxes, etc., which are possible to explain with kinetic modeling. In particular, contour plots of the proton VDF measured around 0.3 AU by Helios showed the nonthermal tails and sometimes also separate bumps on tails (proton beams) formed at low radial distances (Marsch *et al.*, 1982; Marsch, 2006).

Our simulation results demonstrate that the kinetic-scale Alfvénic turbulence can create the nonthermal tails in the proton VDFs in the direction of the local

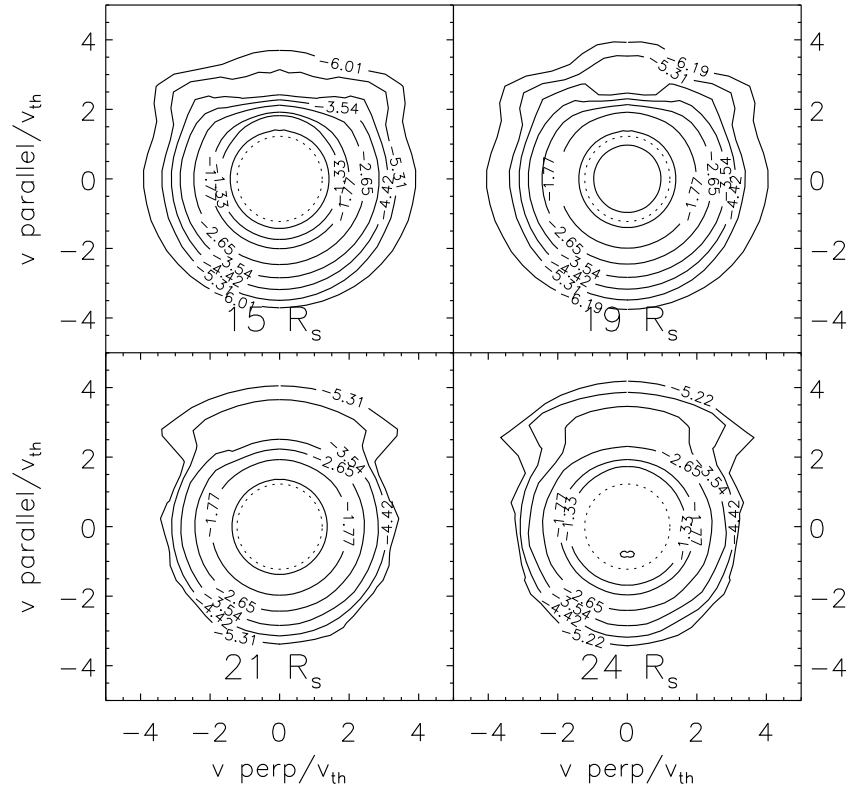


Figure 4. Isocontours of the proton VDF obtained at different radial distances assuming a displaced Maxwellian as boundary condition at $14 R_s$. The evolution equation was solved numerically and included the Fokker-Planck diffusion terms due to turbulence.

magnetic field. The temperature anisotropy of the core is not obtained with this term, but could be by including the 2D diffusion term associated to KAW.

9. Conclusions

An essential difference between MHD and kinetic modeling is the ability of the latter to capture processes of the collisionless wave-particle interactions. Kinetic effects are of particular importance in weakly and mildly collisional media, like solar and stellar coronae and winds, planetary magnetospheres, and interstellar medium. In particular, permanently observed kinetic-scale Alfvénic turbulence need to be incorporated in kinetic solar wind modeling.

We investigated numerically the influence of the kinetic-scale Alfvénic turbulence on the evolution of the proton distribution function and the principal moments in the SW at low radial distances. The effects of the Coulomb collisions

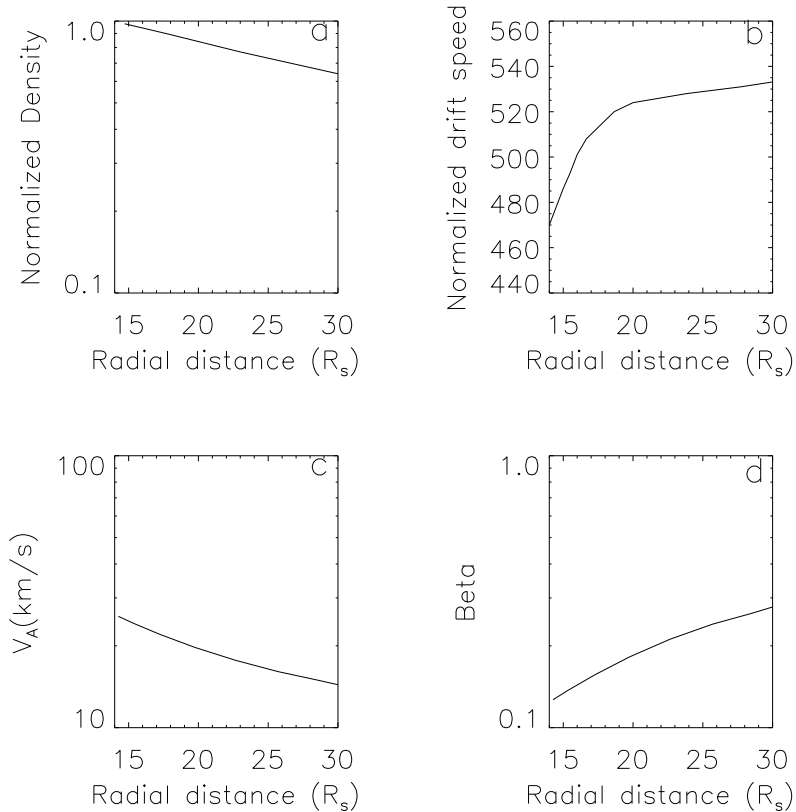


Figure 5. Radial profiles of (a) number density, (b) bulk velocity, (c) the Alfvén velocity, and (d) the plasma beta function. Panels (a) and (b) are obtained by integrating the proton VDF weighted by 1 and V_z , respectively. Kinetic Alfvén turbulence has been taken into account in the evolution equation assuming a displaced Maxwellian as boundary condition at $14 R_s$.

and external forces are compared to those included also turbulence. Observed properties of Alfvénic turbulence are taken into account, including spectral breaks, variable spectral slopes, and radial dependence of the turbulence level. We found significantly different proton VDFs with and without turbulence. In particular, the obtained simulation results demonstrate that the Alfvénic turbulence with characteristics typical for the solar wind is very efficient in producing the nonthermal tails in the proton VDFs in the direction of the background magnetic field. We observed in our simulations a fast generation of the nonthermal proton tails at the heliocentric distances less than 0.3 AU. The tails do not appear without turbulence terms. This provides a natural explanation for the proton VDF with tails routinely observed in situ at 0.3-1 AU.

The turbulence effects on the number density and bulk velocity are also investigated. It is shown that the turbulence has a non negligible influence on

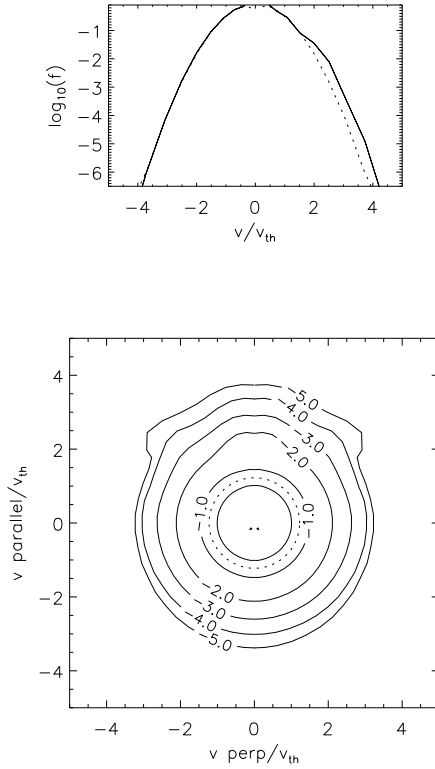


Figure 6. VDF obtained at $30 R_s$ assuming a displaced Maxwellian as the boundary condition at $14 R_s$ by solving the evolution equation including the Fokker-Planck diffusion term due to kinetic Alfvén turbulence. Top panel: Parallel (solid line) and perpendicular (dotted line) cross section of the proton VDF. Bottom panel: Isocontours of the proton VDF in the velocity plane centered on the bulk velocity.

the bulk velocity and increases it in the formation region of the proton tails. On the contrary, the particle number density decreases when the turbulence is accounted for.

In this first kinetic simulation we considered a simplest case of the turbulence spectrum with a single spectral kink, which did not allow us to study the influence of steeper spectra with indices $\delta_{\perp} \propto 3 - 4$ often observed in the solar wind. Again, we used a simplest 1D version of the diffusion coefficient reduced by the averaging in the cross-field velocity plane.

The bump-in-the tail VDFs of protons (proton beams), observed in the solar wind, are not easy to reproduce by the stationary Fokker-Planck diffusion. As is explained in our accompanying paper (Voitenko and Pierrard, 2012), a time-varying diffusion can lead to the beam formation by the time-of-flight effects. The beams can be also produced by the proton trapping and acceleration in

the parallel electric potential of the intermittent KAW pulses, as is explained by Pierrard and Voitenko (2010) and demonstrated numerically by Li *et al.* (2010). Simulation of this process requires a more complex modeling of the solar wind turbulence including intermittence. This work is in progress.

Acknowledgements The research leading to these results has received funding from the Belgian Federal Science Policy in the framework of the program Interuniversity Attraction Pole for the project P7/08 CHARM and from the European Commission's FP7 Program for the STORM (313038) and SWIFF projects (263340, swiff.eu). We thank the referee for his useful suggestions.

References

- Alexandrova, O., Saur, J., Lacombe, C., Mangeney, A., Mitchell, J., Schwartz, S. J., Robert, P.: 2009, *Phys. Rev. Lett.* **103**, 165003.
- Alexandrova, O., Saur, J., Lacombe, C., Mangeney, A., Schwartz, S. J., Mitchell, J., Grappin, R., Robert, P.: 2010, In: Maksimovic, M., Issautier, K., Meyer-Vernet, N., Moncuquet, M., Pantellini, F. (eds.), *Twelfth International Solar Wind Conference, AIP Conf. Proc.* **1216**, 144.
- Bavassano, B., Dobrowolny, M., Mariani, F., Ness, N. F.: 1982, *J. Geophys. Res.* **87**, 3617.
- Cranmer, S.R., van Ballegoijen, A.A.: 2003, *Astrophys. J.* **594**, 573.
- Cranmer, S.R., van Ballegoijen, A.A., Edgar, R.J.: 2007, *Astrophys. J. Suppl.* **171**, 520.
- Hasegawa, A., Chen, L.: 1976, *Phys. Fluids*, **19**, 1924.
- He, J., Marsch, E., Tu, C., Yao, S., Tian, H.: 2011, *Astrophys. J.* **731**, 85.
- He, J., Tu, C., Marsch, E., Yao, S.: 2012, *Astrophys. J.* **745**, L8.
- Hinton, F. L.: 1983, In: Galeev, A.A., Sudan, R.N. (eds), *Basic Plasma Physics I and II*, North-Holland, New-York, 148.
- Lamy, H., Pierrard, V., Maksimovic, M., Lemaire, J.: 2003, *J. Geophys. Res.* **108**, 1047.
- Lemaire, J., Pierrard, V.: 2001, *Astrophys. Space Sci.* **277**, 2, 169.
- Li, X., Lu, Q., Chen, Y., Li, B., Xia, L.: 2010, *Astrophys. J. Lett.* **719**, L190.
- Lie-Svendsen, O., Hansteen, V.H., Leer, E.: 1997, *J. Geophys. Res.* **102**, 4701.
- Lie-Svendsen, O., Leer, E.: 2000, *J. Geophys. Res.* **105**, 35.
- Maksimovic, M., Pierrard, V., Lemaire, J.: 1997, *Astron. Astrophys.* **324**, 725.
- Marsch, E.: 2006, *Living Rev. Solar Phys.* **3**(1), <http://www.livingreviews.org/lrsp-2006-1>.
- Marsch, E., Mulhauser, K.-H., Schwenn, R., Rosenbauer, H., Pilipp, W., Neubauer, F.: 1982, *J. Geophys. Res.* **87**, 52.
- Osmane, A., Hamza, A. M., Meziane, K.: 2010, *J. Geophys. Res.* **115**, A05101.
- Parker, E.N.: 1958, *Astrophys. J.* **128**, 664.
- Pierrard, V.: 2011, In: Pogorelov, N.V. (ed.), *5th International Conference of Numerical Modeling of Space Plasma Flows, ASP Conf. Ser.* **444**, 166.
- Pierrard, V., Lazar M., and Schlickeiser R.: 2011, *Solar Phys.* **269**, 421.
- Pierrard, V., Lemaire, J.: 1996, *J. Geophys. Res.* **101**, 7923.
- Pierrard, V., Lemaire, J.: 1998, *J. Geophys. Res.* **103**, 11701.
- Pierrard, V., Maksimovic, M., Lemaire, J.: 1999, *J. Geophys. Res.* **104**, 17021.
- Pierrard, V., Maksimovic, M., Lemaire, J.: 2001, *J. Geophys. Res.* **107**, 29305.
- Pierrard, V., Voitenko, Y.: 2010, In: Maksimovic, M., Issautier, K., Meyer-Vernet, N., Moncuquet, M., Pantellini, F. (eds.), *Twelfth International Solar Wind Conference, AIP Conf. Proc.* **1216**, 102.
- Podesta, J.J., Gary S.P.: 2011, *Astrophys. J.*, **734**, 15.
- Vocks, C., Mann, G.: 2003, *Astrophys. J.* **593**, 1134.
- Vocks, C., Mann, G.: 2009, *Astron. Astrophys.* **502**, 325.
- Voitenko, Y., Goossens, M.: 2006, *Space Sci. Rev.*, **122**, 255.
- Voitenko, Y., Pierrard, V.: 2012, *Solar Phys.*, submitted.